Electron-nuclear spin dynamics in a bacterial photosynthetic reaction center

Daviso, E.; Alia, A.; Prakash, S.; Diller, A.; Gast, P.; Lugtenburg, J.; … ; Jeschke, G.

Electron−Nuclear Spin Dynamics in a Bacterial Photosynthetic Reaction Center

Eugenio Daviso,[†] A. Alia,[†] Shipra Prakash,[†] Anna Diller,[†] Peter Gast,[‡] Johan Lugtenburg,[†] Jörg Matysik,*,[†] and Gunnar Jeschke[§]

Leiden Institute of Chemistry, Einsteinweg 55, P.O. Box 9502, 2300 RA Leiden, The Netherlands, Leiden Institute of Physics, Niels Bohrweg 2, P.O. Box 9504, 2300 RA Leiden, The Netherlands, Laboratorium für Physikalische Chemie, Eidgenössische Technische Hochschule Zürich, Hönggerberg, 8093 Zürich, Switzerland

The solid-state photo-CIDNP effect is known to occur in natural photosynthetic reaction centers (RCs) where it can be observed by magic-angle spinning (MAS) NMR as strong modification of signal intensities under illumination compared to experiments performed in the dark. The origin of the effect has been debated. In this paper, we report time-resolved photo-CIDNP MAS NMR data of reaction centers of quinone depleted *Rhodobacter sphaeroides*. It is demonstrated that the build-up of nuclear polarization on the primary donor and the bacteriopheophytin acceptor depends on the presence and lifetimes of the molecular triplet states of the donor and carotenoid. Analysis of the data proves that up to three electron−nuclear spin-coupling mechanisms and two transient effects are working concomitantly in the spin-chemical machinery of the reaction center.

Introduction

The observation of the change of triplet yield in bacterial reaction centers (RCs) upon variation of the external magnetic field[1,2] was the discovery of the first magnetic field effect (MFE) occurring in a photosynthetic system. In a later study, the observation was confirmed and extended to higher magnetic fields up to 5 T.[3] A linkage between this hyperfine driven phenomenon and the photochemically induced dynamic electron polarization (photo-CIDEP), which is observed by electron paramagnetic resonance (EPR) spectroscopy as strong modification of signal intensities under illumination compared to experiments performed in the dark, was seen immediately (for review, see refs 4, 5). Later, it was shown that the MFE in photosynthetic RCs is anisotropic[3] and temperature dependent.[6] Inspired by the radical-pair mechanism (RPM),[7,8] known at that time from photo-CIDNP in liquid-state NMR,[9,10] electron−nuclear interactions were recognized as source of the MFE and "the possibilities of new categories of experiments"[11] were foreseen. The RPM in the solid state is not sufficient to explain nuclear polarization on the primary donor and the bacteriopheophytin acceptor build up because anisotropic contributions of the hyperfine interaction (hfi) $\Delta A = A_{zz} - (A_{xx} + A_{yy})/2$ and the fixed electron−electron coupling lead to additional mechanisms for polarization generation.[12,13] Furthermore, the RPM is based on the diffusion of the radicals so that nuclear polarization from the singlet (S) and triplet (T_0) radical states is not canceled out. Here we aim for completing the understanding of the character of the electron−nuclear interactions occurring in the solid state.

The discovery of the solid-state photo-CIDNP effect by Zysmilich and McDermott in 1994 in frozen and quinone-blocked bacterial RCs of *Rhodobacter* (*Rb.*) *sphaeroides* R26 by ^{15}N MAS NMR under continuous illumination with white

light first allowed study of the effects of electron−electron nuclear dynamics by observation of individual nuclei rather than the electrons.[14] In recent years, photo-CIDNP has been observed also with ^{13}C MAS NMR and on various photosynthetic RCs, as those of the purple bacteria *Rb. sphaeroides* wild-type (WT)[15] and its carotenoid-less mutant R26,[16,17] of the green sulfur bacterium *Chlorobium tepidum*,[18] of heliobacterium *Heliobacillus mobilis*,[19] as well as of the plant photosystems I and II.[20−22]

In RCs of *Rb. sphaeroides*, light induces electron charge separation within 3 ps from the special pair P to the bacteriopheophytin Φ (Figure 1), which is the primary acceptor, neglecting a putative very short-lived state with the electron localized at the accessory chlorophyll.[23] The lifetime of the accessory chlorophyll intermediate is too short for nuclear polarization to be built up. The spin-correlated radical pair P[•+] Φ[•−] is born in a pure singlet state (Figure 2) inducing photo-CIDEP observed as strong absorptive and emissive signals in EPR. During the lifetime of the radical pair, the electron−spin system oscillates between the S and the T_0 states at a frequency dependent both on the secular part of the hfi A_{zz} and on the difference of the electron Zeeman frequencies $\Delta\Omega$ of the radical pair. In the solid state, this oscillation is slightly modified by the nonsecular part of the hyperfine coupling, the dipole−dipole coupling between the two electrons and the exchange coupling. The probability to find the radical pair in a S or T_0 state depends on the sign of the nuclear magnetic quantum number. This is one important ingredient of the RPM in liquids, and the sign rules for this process can be found elsewhere.[24]

Three mechanisms have been proposed to explain the origin of the asymmetric build up of nuclear polarization from the two decay channels (Figure 2) leading to the net ground-state polarization under continuous illumination experiments:[12,25]

(i) In the electron−electron nuclear three-spin mixing (TSM) mechanism, the symmetry of the coherent spin evolution in the correlated radical pair is broken by state mixing due to anisotropic electron−electron dipolar coupling and pseudosecular hf coupling.[26] The symmetry breaking concerning the nuclear states is caused by the pseudosecular hf coupling, which

* To whom correspondence should be addressed. E-mail: j.matysik@chem.leidenuniv.nl. Phone: +31-71-5274198. Fax: +31-71-5274603.
[†] Leiden Institute of Chemistry.
[‡] Leiden Institute of Physics.
[§] Laboratorium für Physikalische Chemie, Eidgenössische Technische Hochschule Zürich.
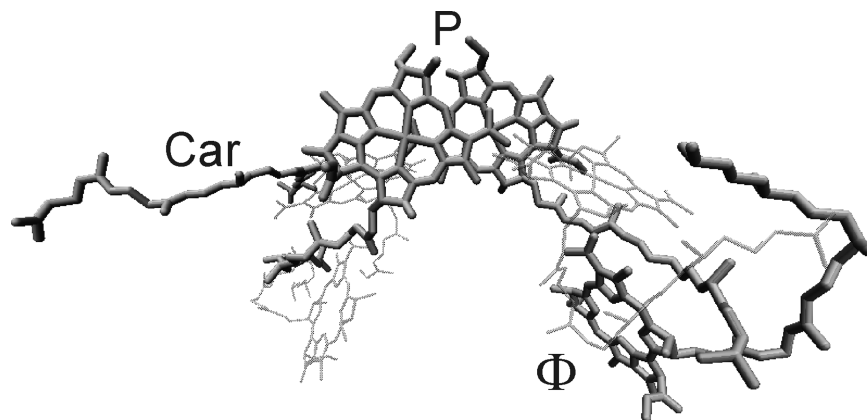
Figure 1. Cofactors involved in primary charge separation and recombination of the bacterial reaction center of *Rb. sphaeroides* wild type showing the special pair P, which is the primary donor formed by two bacteriochlorophylls *a* P_L (right) and P_M (left), the primary electron acceptor Φ, a bacteriopheophytin *a*, and the carotenoid Car. Other cofactors are shown in light gray.
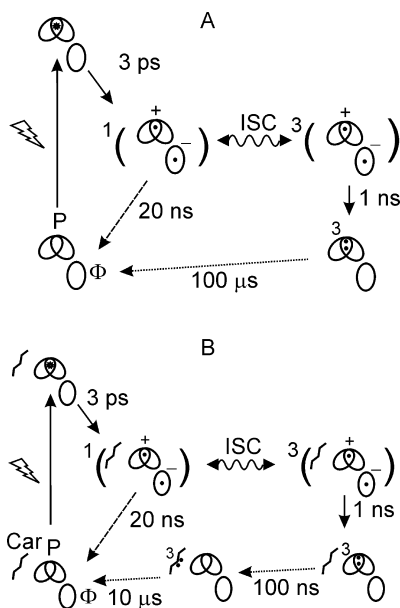
Figure 2. Kinetics and spin dynamics of electron transport in quinone-depleted RCs of *Rb. sphaeroides* wild type and the carotenoid-less strain R26. (A) R26. After absorption of a single photon from the photochemically excited-state of the primary donor P*, an electron is transferred to the primary acceptor Φ, a bacteriopheophytin cofactor. This initial singlet radical pair $^1(P^{\bullet+}\Phi^{\bullet-})$ is a nonstationary state and can be represented as a polarized fictitious electron spin state. An electron back-transfer leads to the initial electronic ground state. Because of hf interaction with nuclei, the singlet radical pair evolves into a triplet radical pair $^3(P^{\bullet+}\Phi^{\bullet-})$. Concomitantly to this process of spin intersystem crossing (ISC), electron polarization is transferred to nuclei by the TSM and by the DD mechanisms. *Net* nuclear polarization is produced by unbalancing the decay pathways of the singlet and the triplet radical pair (singlet and triplet branch). In RCs having a long lifetime of the donor triplet, as in R26 RCs, the DR occurs because nuclear spin relaxation is significant on the triplet decay pathway (triplet branch), causing incomplete cancelation of nuclear polarization from both decay pathways. The nuclear DR occurs only at the donor side P. (B) Wild type. Scheme for charge separation of the donor followed by quenching of the carotenoid leading to a triplet excited-state having a lifetime of ~7.5 μs. The dashed arrows indicate path and timing of the transient nuclear polarization (TNP) generated in the singlet radical state and detected in the ground state. The dotted arrows indicate path and timings of the transiently obscured polarization (TOP) induced by paramagnetic triplets. Only steady-state nuclear polarization remains observable after the excited triplet states have decayed to the ground state.

tilts the quantization axes of nuclear spins with respect to the external magnetic field. The tilt angles and tilt direction differ in the electron spin α and β manifold.[27] This tilt converts part of the electron−electron zero-quantum coherence that exists in a single-born radical pair to electron−electron nuclear zero/single quantum coherence. A further tilt of the electron spin quantization axes by the exchange coupling or by the pseudosecular component of the electron−electron dipole−dipole coupling converts part of this three-spin coherence to nuclear antiphase coherence. This corresponds to a symmetry breaking with respect to the single and triplet state of the radical pair. The antiphase nuclear coherence evolves to nuclear coherence during the lifetime of the radical pair. When the radical pair recombines, the hyperfine coupling and electron−electron coupling become zero, the tilt of all quantization axes vanishes, and the nuclear coherence is partially converted to nuclear polarization.

(ii) In the electron−nuclear differential decay (DD) mechanism, the first symmetry breaking with respect to nuclear spin states is induced by pseudosecular hf coupling in the same way as in the TSM mechanism. The symmetry with respect to the S and T_0 states of the pair is broken by different lifetimes of these states.[13] Electron−electron zero-quantum coherence thus acquires a phase-dependent lifetime, as the S and T_0 states correspond to different phase of this coherence. For the electron−electron-nuclear zero/single quantum coherence, the phase evolution of electron−electron zero-quantum coherence is correlated with phase evolution of nuclear coherence. Recombination of the radical projects nuclear coherence to nuclear polarization. As the probability for this recombination is correlated with the phase of the nuclear coherence, net polarization is generated.

(iii) In the differential relaxation (DR) mechanism, nuclear polarization in the triplet decay pathway is depleted by paramagnetic longitudinal relaxation during the lifetime of the donor triplet ^3P. Therefore, the nuclear polarization of the triplet decay channel can not longer fully offset the polarization from the singlet decay pathway, and net nuclear polarization is produced.[11,28] This third mechanism is not expected to be relevant in WT RCs having a ^3P lifetime of about 100 ns.[15] The longitudinal relaxation is induced by fluctuations of the anisotropic part of the hyperfine coupling in the triplet state, which are in turn induced by molecular motion of the chlorophyll macrocycle plane. Generally this relaxation can be treated by Solomon theory.[29] According to this theory, polarization from the DR mechanism is proportional to the square of the anisotropy of the hyperfine coupling T^2 in the triplet state. NMR signal patterns for this mechanism can be computed with a single

Electron−Nuclear Spin Dynamics in Bacterial RCs

J. Phys. Chem. C, Vol. 113, No. 23, 2009 **10271**

TABLE 1: Selected NMR ^{13}C Chemical Shifts Assigned to P_M, P_L, and Φ in the Literature and the Ones Used to Fit Time-Resolved Natural Abundance *Rb. sphaeroides* R26 Spectra

IUPAC no.	chemical shift (ppm)	chemical shift this work (ppm)
C19-P_M	162.5[a]	163.1
C10-Φ	101.6[b]	100.7
C7^1-P_L		24.1
C6-P_L	164.6[a]	164.1
C9-P_L	161.0[c]	160.8
C15-P_M	106.8[c]	106.8

[a] See ref 30. [b] See ref 31. [c] See ref 17.

TABLE 2: Selected NMR ^{13}C Chemical Shifts Assigned to P_M, P_L, and Φ in the Literature and the Ones Used to Fit Time-Resolved 4-ALA *Rb. sphaeroides* Wild Type Spectra

| IUPAC no.	chemical shift (ppm)	chemical shift this work (ppm)
C11-P_L	154.2[a]	153.3
C19-P_L	159.7[a]	159.8
C19-Φ	170.2[a]	170.0
C13-P_M	131.0[a]	132.6
C6-P_L	164.6[a]	164.0
C8-Φ	54.9[a]	54.6

[a] See ref 30.

free fit parameter, which is related to the product of the correlation time and angular amplitude of the molecular motion. Prediction of this parameter is currently impossible for a system that is on the verge of a transition between a soft matter and glassy state. Furthermore, a full theory would have to take into account relaxation on forbidden electron−nuclear transitions. Such relaxation is also proportional to T^2, but the time scale may be set by other motional processes. Therefore, nuclear polarization induced by the DR mechanism currently cannot be predicted ab initio. However, spectra can be simulated satisfyingly by fitting only a single parameter related to the dynamics of the system.[17]

In all these mechanisms, the *net* nuclear polarization in the ground state corresponds to the sum of both polarizations generated in the S and in the T$_0$. All experimental results obtained to date by steady-state experiments are matching well with the assumption that TSM and DD mechanisms are contributing to nuclear polarization build up during the lifetime of the radical pair while DR mechanism requires the long living ^{3}P of R26.[15,17] However, because of uncertainties of the ^{13}C hf tensors and the contribution of spin-diffusion processes to steady-state polarizations, no quantitative prediction of the spectra is possible.

Here we present ^{13}C photo-CIDNP MAS NMR experiments of both RCs from *Rb. sphaeroides* WT and R26 with time resolution in the microsecond to millisecond range. These experiments provide a much more critical test for the theory and, in addition, give more direct access to electron−nuclear interactions in the highly optimized photosynthetic systems.

Experimental Methods

Sample Preparation and NMR Measurements. The detergent solubilized quinone depleted RCs of *Rb. sphaeroides* of natural abundance (n.a.) WT has been prepared as in ref 15. Preparation of detergent solubilized, quinone depleted, and 4-^{13}C-δ-aminolevulinic acid (4-ALA) labeled RCs of *Rb. sphaeroides* WT is reported in ref 30. The detergent solubilized quinone depleted RCs of *Rb. sphaeroides* of n.a. R26 has been prepared as in ref 31.
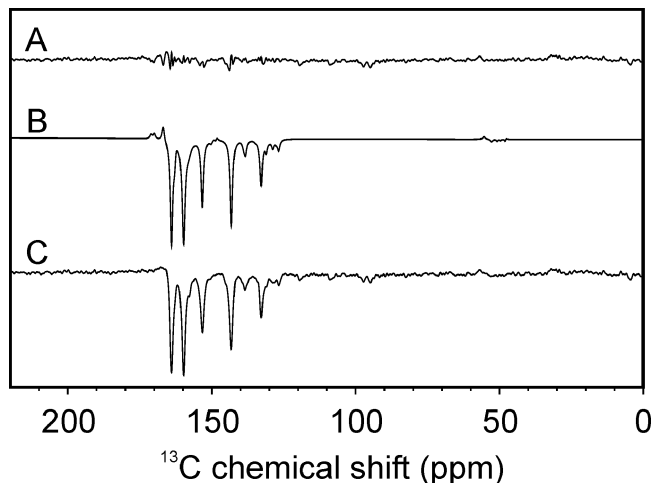
Figure 3. Example of a fitted spectrum of RCs (A) Residual spectrum obtained from B−C. (B) Deconvoluted spectrum of C. (C) Photo-CIDNP MAS NMR spectrum of wild type 4-ALA labeled in which laser light excitation was followed by NMR detections with a delay of 80 μs.

TABLE 3: Parameters of Fits of the Time Evolution of Nuclear Polarization by First-Order Kinetics for Selected ^{13}C Nuclei in P_M, P_L, and Φ of 4-ALA Labeled *Rb. sphaeroides* Wild Type

| IUPAC no.	a	b	τ_B (s)
C11-P_L	−0.13 ± 0.03	−0.45 ± 0.03	10.90 ± 2.0
C19-P_L	−0.24 ± 0.03	−0.70 ± 0.04	8.91 ± 0.98
C19-Φ	0.14 ± 0.01	−0.08 ± 0.01	9.86 ± 2.43
C13-P_M	−0.30 ± 0.01	0.25 ± 0.01	9.30 ± 0.61
C6-P_L	−0.13 ± 0.04	−0.79 ± 0.05	7.88 ± 1.05
C8-Φ	−0.22 ± 0.03	−0.13 ± 0.01	11.78 ± 1.15

TABLE 4: Parameters of Fits of the Time Evolution of Nuclear Polarization by First-Order Kinetics for Selected ^{13}C Nuclei in P_M, P_L, and Φ of Natural Abundance *Rb. sphaeroides* R26

IUPAC no.	a	b	τ_B (s)
C19-P_M	0.52 ± 0.02	−0.21 ± 0.02	97.13 ± 32.08
C10-Φ	−0.22 ± 0.01	−0.12 ± 0.01	114.20 ± 26.52
C7^1-P_L	0.33 ± 0.01	−0.33 ± 0.01	88.11 ± 10.60
C6-P_L	0.62 ± 0.01	−0.32 ± 0.02	45.30 ± 12.47
C9-P_L	0.92 ± 0.06	−0.47 ± 0.07	75.44 ± 38.52
C15-P_M	−0.33 ± 0.02	0.17 ± 0.02	56.69 ± 24.22

Time-resolved ns-flash photo-CIDNP MAS NMR measurements have been performed as described in ref 32 by changing the delay time between laser light pulse excitation and NMR detection systematically from 0 to 100 μs in *Rb. sphaeroides* WT n.a. and 4-ALA RCs, and from 0 to 800 μs in *Rb. sphaeroides* R26 n.a.. In all experiments, temperature was kept at 233 K.

Spectral Fitting and Nuclear Polarization Evolution. The fitting of the spectrum collected using time-resolved MAS NMR photo-CIDNP of pure RCs of *Rb. sphaeroides* R26 was performed using Igor Pro v. 6.01 (Lake Oswego, Oregon). The peaks are Lorentzian, with a full width at half-height of 40−60 Hz as experimentally observed using the 4-ALA labeling pattern of *Rb. sphaeroides* WT.[30] The chemical shifts and their ^{13}C correlations have been compared to the values taken from the literature in Tables 1 and 2. During the fitting procedures, the chemical shifts were kept fixed for all the spectra collected at different time scales. A typical spectral fitting result is shown in Figure 3. Fitting of the time-resolved photo-CIDNP as a function of the build up time was performed for both sets of
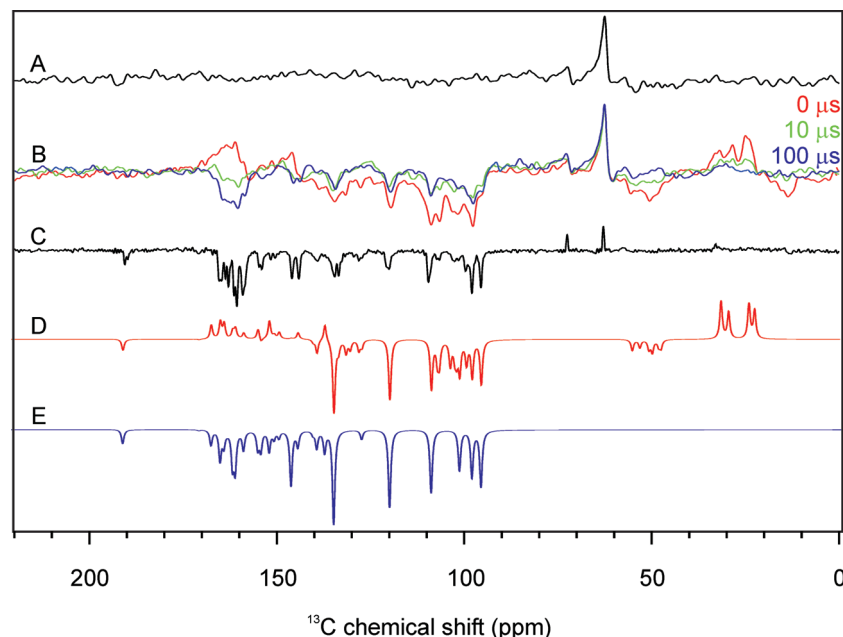
Figure 4. ^{13}C photo-CIDNP MAS NMR spectra of ^{13}C natural abundance RCs of *Rb. sphaeroides* wild type, (A) in the dark, (B) with laser flashes, and (C) under continuous illumination with white light. Traces (B) are spectra obtained at three different time delays between the light pulse and the NMR detection pulse (red 0 μs, green 10 μs, and blue 100 μs) using 532 nm 8 ns flashes. All the spectra have been collected at a magnetic field of 4.7 T and a temperature of 233 K. The simulated spectrum (D) shows the transient nuclear polarization occurring in the singlet state of the radical pair due to isotropic (similar to RPM) and anisotropic contributions (TSM and DD). Transiently obscured polarization (TOP) induced by the paramagnetic triplet state of the carotenoid has been considered by subtraction of 10% of the triplet polarization in the ground state. The simulated spectrum (E) shows polarization in the ground state of the RC generated via the singlet and triplet states of the radical pair due to anisotropic hf contribution (TSM and DD).

data, 4-ALA WT and natural abundance R26, using the following expression for first-order kinetics:

$$y = a + b(1 - e^{-x/\tau_\mathrm{B}}) \qquad (1)$$

where y is the nuclear polarization as a function of the delay time between the excitation light pulse and NMR detection time x. The constant τ_B gives information on the time scale of the photo-CIDNP intensities build up as detected by NMR (Tables 3 and 4).

Numerical Simulations. Numerical simulations of the photo-CIDNP effect were based on the theory described in refs 12, 25 as implemented in a home written Matlab program for density matrix computation using the EasySpin library.[33] The program starts from a pure singlet state of the pair and computes time evolution under a Hamiltonian including electron Zeeman, nuclear Zeeman, and hf interaction as well as dipole−dipole and exchange coupling between the two electron spins.[12,25] The part of the density matrix that decays to the ground state from the S and to the ^{3}P from the T$_0$ is projected out and further evolved under a Hamiltonian including only the nuclear Zeeman interaction.

For WT RCs, the computed total nuclear polarization at the end of the photocycle is the sum of the polarization arising from the singlet branch and from the triplet branch obtained by neglecting any contribution caused by the DR mechanism. The lifetime of the ^{3}P (Figure 2B) is too short to permit significant nuclear paramagnetic relaxation. For R26 systems, paramagnetic relaxation in the ^{3}P as well as the return to the ground state are simulated based on differential kinetic equations[34] assuming first-order kinetics for both processes. This procedure is performed for a full powder average, describing all interactions by tensors. A spherical grid, function *sphgrid* in EasySpin,[33] with 16 knots and C_i symmetry (481 orientations), has been found to be sufficient for powder averaging.

Nuclear polarization was normalized to the thermal polarization at the measurement temperature of 233 K. The computed photo-CIDNP intensities obtained at different timings of the photocycle have been used as input file for Spinevolution.[35] An example of the script used to simulate the spin−echo MAS NMR spectra of the RC of *Rb. sphaeroides* R26 is available in the Supporting Information (Figure 4, traces D and E, Figure 5, traces D and E, Figure 6, traces D and E). The evolution of nuclear polarization for 4-ALA WT (Figure 7D,D′) and of R26 (Figure 7 B,B′) have been obtained in Matlab. For simulations of Figure 7B,B′,D,D′, no scaling factors were used. Nuclear polarization has been evaluated following the same general mechanisms (TSM, DD, and DR) at different time scales of NMR detection for WT (0−80 μs) and R26 (0−800 μs). The curves of the nuclear polarization have not been shifted relative to each other, and their values are the absolute values of the output of the computations. Only the y-axis of the simulated data have been chosen for convenient comparison to the experimental data (Figure 7A,A′,C,C′). Differences between experimental and simulated data are mainly due to imprecision of DFT calculations as well as the estimation of the g tensor of the bacteriopheophytin acceptor. Furthermore, the error margins are rather large for the exchange and the electron−electron dipole coupling in the radical pair. For details, see Supporting Information.

DFT Calculations of Hyperfine Tensors. DFT computations of hf coupling tensors were performed with the ADF 2002.1 package (SCM NV, Amsterdam, The Netherlands), using the TZP all-electron basis set for all atoms as described before.[17] Geometries of ground-state molecules were taken from the crystal structure in the charge-neutral state (PDB identifier 1AIJ)[36] and subjected to geometry optimization within ADF in the cation radical state in vacuo. Such geometry optimization converges to the local minimum of the energy hypersurface that

Electron−Nuclear Spin Dynamics in Bacterial RCs

J. Phys. Chem. C, Vol. 113, No. 23, 2009 **10273**
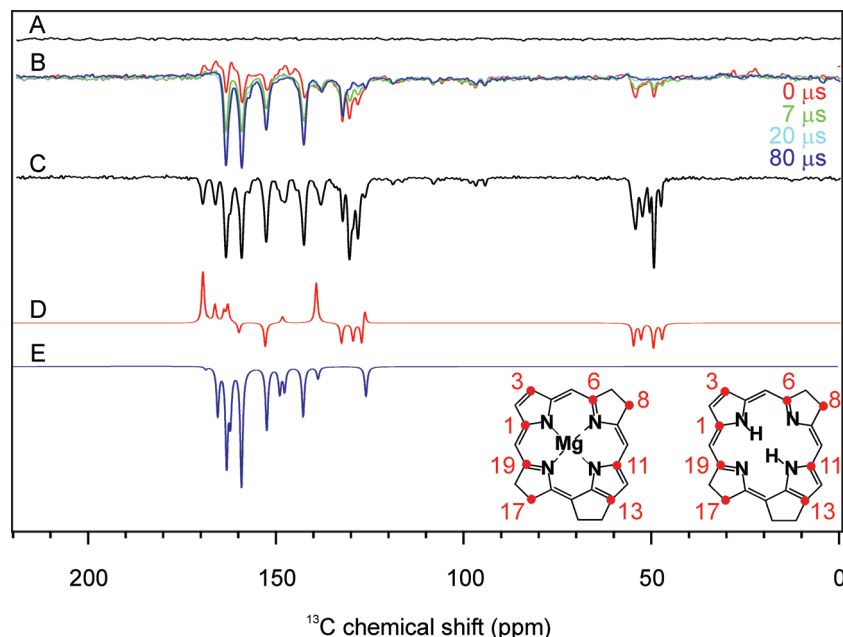
Figure 5. ^{13}C photo-CIDNP MAS NMR spectra of 4-ALA ^{13}C labeled RCs of *Rb. sphaeroides* wild type (A) in the dark, (B) with laser flashes, and (C) under continuous illumination with white light. Traces (B) are spectra obtained at four different time delays between the light pulse and the NMR detection pulse (red 0 μs, green 7 μs, light-blue 20 μs, and dark-blue 80 μs) using 532 nm 8 ns flashes. All the spectra have been collected at a magnetic field of 4.7 T and a temperature of 233 K. The simulated spectrum (D) shows the transient nuclear polarization occurring in the singlet state of the radical pair due to isotropic (similar to RPM) and anisotropic contributions (TSM and DD). Transiently obscured polarization (TOP) induced by the paramagnetic triplet state of the carotenoid has been considered by subtraction of 10% of the triplet polarization in the ground state. The simulated spectrum (E) is the ground-state nuclear net polarization of both states of the radical pair due to the anisotropic contribution (TSM and DD). The inset shows the specific ^{13}C isotope labeled pattern in a bacteriochlorophyll *a* (left) and bacteriopheophytin *a* (right) molecule. Side chains are omitted.
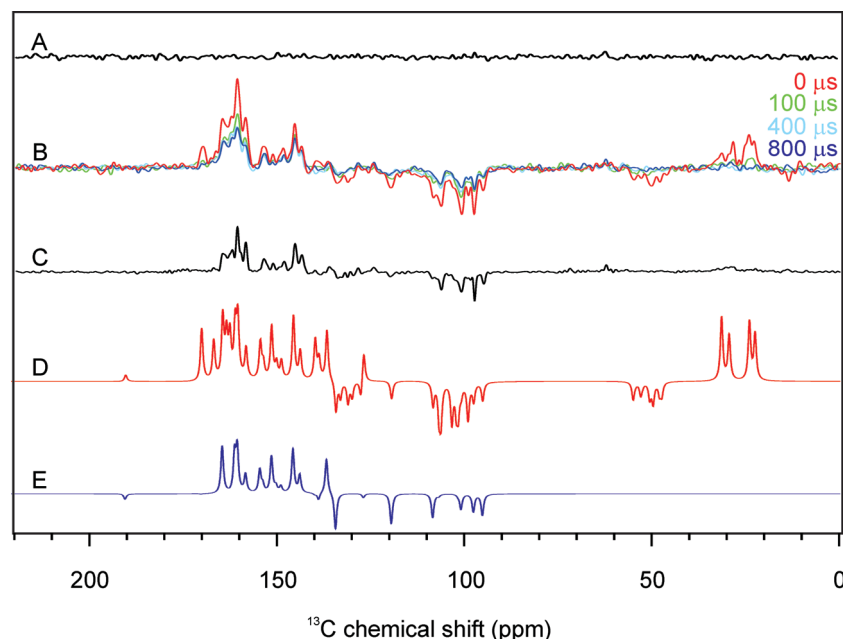

Figure 6. ^{13}C photo-CIDNP MAS NMR spectra of ^{13}C natural abundance RCs of *Rb. sphaeroides* R26 obtained (A) in the dark, (B) with laser flashes and (C) under continuous illumination with white light (C). Traces B are spectra obtained at four different time delays between the light pulse and the NMR detection pulse (red 0 μs, green 100 μs, light blue 400 μs and dark blue 800 μs) using 532 nm 8 ns flashes. All the spectra have been collected at a magnetic field of 4.7 T and a temperature of 233 K. The simulated spectrum (D) shows the transient nuclear polarization occurring in the singlet state of the radical pair mainly due to isotropic contributions. The simulated spectrum (E) is the resulting nuclear net polarization of both states of the radical pair due to the anisotropic contribution (TSM, DD, and DR).

is next to the experimental structure, so that side group conformations and deformations of the macrocycles are preserved. The hf computations were performed considering P_L and P_M coordinated with His-L173 and His-M202 to the Mg atom and with the phytyl chain substituted by a methyl group. The computed hyperfine tensors of the bacteriochlorophylls

forming the primary donor and the bacteriopheophytin acceptor are reported in Tables S1, S2, and S3 of the Supporting Information.

DFT Calculations of *g* Tensors. To obtain principal axis directions of the *g* tensors, spin-restricted spin−orbit relativistic computations were performed within the ZORA formalism[37] as
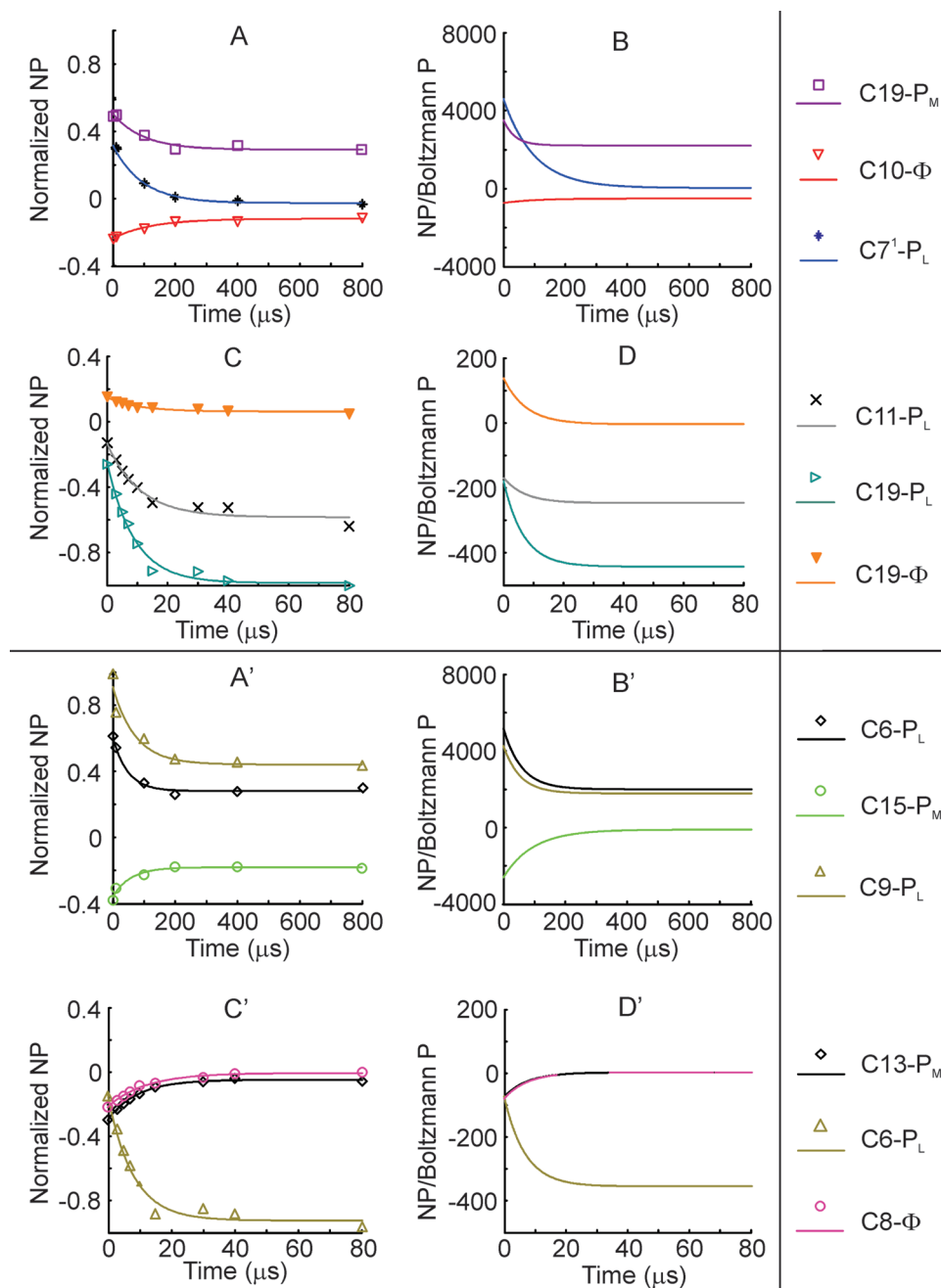
Figure 7. (A–A′) Normalized NMR intensities plotted as a function of the delay time between the light pulse and the NMR detection pulse for selected ^{13}C resonances from natural abundance RCs of *Rb. sphaeroides* R26. For numbering and assignment of the carbons, see Table 1. The fit reveals that the polarization evolution can be described by first-order kinetics with an average time constant of about 80 μs. (B–B′) Simulated evolution of nuclear polarization for selected ^{13}C resonances from RCs of *Rb. sphaeroides* R26 at natural abundance considering action of the TSM, DD and DR mechanisms. A triplet lifetime of 75 μs was assumed. (C–C′) Normalized NMR intensities plotted as a function of the delay time between the light pulse and the NMR detection pulse for selected ^{13}C resonances from RCs of *Rb. sphaeroides* wild type labeled with 4-ALA. For numbering and assignment of the carbons, see Table 2. The fit reveals that the polarization evolution constant has a value between 5 and 10 μs. (D–D′). Simulated evolution of nuclear polarization for selected ^{13}C resonances from RCs of *Rb. sphaeroides* wild type labeled with 4-ALA considering parallel action of the TSM and DD mechanisms. Triplet lifetimes of 100 ns for the majority fraction and 7.5 μs for the minority fraction were assumed. The fraction of RCs with carotenoid triplets was adjusted to give the best agreement with experiment resulting at a value of ~10%.

implemented in the ADF 2002.1 package (SCM NV, Amsterdam, The Netherlands). A TZ2P all-electron basis set was employed for the acceptor anion radical and, because of memory restrictions, a DZP all-electron basis set for the special pair cation radical. In all cases, the BLYP functional was used. The computations were performed, both with the initial geometry taken from the X-ray structure with just the protons added, and with the geometry optimized within ADF. Geometry optimizations were performed with the BLYP functional and frozen-

core basis sets (all electron for hydrogen atoms, first shell frozen for carbon, nitrogen, and oxygen atoms, first two shells frozen for magnesium atoms) at double-ζ level (basis set DZ). For the acceptor anion radical, deviations of the g tensor principal axes between the original and optimized structure at TZ2P level were 6.9°, 20.8°, and 21.8° for g_{xx}, g_{yy}, and g_{zz}, respectively. For the donor cation radical, these deviations at DZP level are 8.7°, 11.5°, and 14.5° for g_{xx}, g_{yy}, and g_{zz}, respectively. For the donor cation radical, the computed principal axis directions could be

Electron−Nuclear Spin Dynamics in Bacterial RCs

J. Phys. Chem. C, Vol. 113, No. 23, 2009 **10275**

compared to the experimental directions.[38] For the *g* tensor computed from the original structure, all three axes deviate by approximately 4° from the corresponding experimental axes, with the experimental errors being ±1−2°. Agreement is slightly worse for the optimized structure, hence the parameters were taken from the computation for the original structure. The *g* tensor principal values (g_{xx}, g_{yy}, g_{zz}) for the donor differ by $(-16.0, -1.37, -1.44) \times 10^{-4}$ between the original and optimized structures, suggesting that these values are much less reliable than the principal axis directions and also much less reliable than experimental *g* tensor principal values from high-field EPR studies. Indeed, deviations from the experimental values[39] are as large as $(27.54, 6.34, -2.68) \times 10^{-4}$. Hence, the experimental values were used for the simulations of spin dynamics and are given in the Supporting Information, Table S4. For the acceptor the differences are $(-1.92, -1.54, -2.24) \times 10^{-4}$ for DFT computations on the original and optimized structure and $(10.7, 6.62, -2.8) \times 10^{-4}$ between the TZ2P DFT computation on the optimized structure and experimental values for the bacteriopheophytin anion radical in *Rhodopseudomonas viridis*.[40] Also, in this case, the experimental principal values were used in simulations and are given in the Supporting Information, Table S5. Principal axis directions, which are not experimentally known for bacteriopheophytin anion radicals, were taken from the computation on the optimized structure, which has smaller deviations in the principal values from the experimental ones.

Basis set dependence was tested for the optimized structure of the acceptor anion radical employing the DZ, DZP, and TZ2P basis sets. All principal axes deviate by no more than 0.7° between different basis sets. The main change (about 0.5°) is between DZP and TZ2P level. The principal values of the g tensor decrease by up to 0.7×10^{-4} when going from the DZ to the DZP basis set and change by 3.4×10^{-4}, 2.2×10^{-4}, and -0.2×10^{-4} when going from the DZP to the TZ2P basis set. This again demonstrates that the principal values are much less reliable than the principal axis directions.

Results and Discussion

^{13}C Photo-CIDNP MAS NMR on WT RCs of *Rb. sphaeroides*. Trace A in Figure 4 is the ^{13}C NMR spectrum of the n.a. WT bacterial RC collected in the dark. The broad peak at 65 ppm originates from the detergent and is due to residual Boltzmann polarization.[32]

Trace B in Figure 4 is the superposition of three ^{13}C MAS NMR spectra of WT RCs obtained at delay times of 0, 10, and 100 μs between an 8 ns laser light pulse with a wavelength of 532 nm and the leading edge of the 5 μs NMR detection pulse. The spectrum obtained with detection immediately after the light pulse (shown in red) exhibits a transient polarization pattern that is similar to the steady-state pattern observed for R26 RCs (see below). The polarized enhanced positive (absorptive) signals have been mainly assigned to P,[30] while the majority of the polarized negative (emissive) signals have been attributed to the Φ.[31] In the spectrum collected at 10 μs (shown in green), the positive donor signals disappear and the negative acceptor signals become weaker. The spectrum obtained at 100 μs (shown in dark-blue) is entirely negative, similar to data known from continuous illumination experiments on WT samples (Trace C in Figure 4).[15] This demonstrates that, after return of all RCs to the ground state, nuclear polarization is dominated by contributions from the TSM mechanism, which have the same sign for the donor and acceptor.[12] In contrast to the TSM contribution, whose sign is independent of the sign of the *g* value difference

Δg, the DD and DR contributions have different sign for donor and acceptor.

To improve the signal, selective isotope labeling on the cofactors has been applied by feeding the bacteria with ^{13}C-labeled 4-ALA. The labeling pattern is shown in the inset of Figure 5.[30] In Figure 5, Trace A shows the dark spectrum of such a selectively isotope labeled sample, and Trace B is the superposition of several ns laser flash photo-CIDNP spectra with the delay times between irradiation and detection varying systematically from 0 to 80 μs. In the initial phase, covering delay times from 0 to 7 μs, positive signals appear in the regions between 140 and 180 ppm as well as between 20 and 40 ppm. This initial positive phase is followed by a phase of entirely negative signals, which is similar to the entirely negative spectrum observed in 4-ALA WT RCs under continuous illumination (trace C in Figure 5),[30,41] although in the steady-state of the labeled sample, spin diffusion occurs, leading to equilibration of signal intensity and to occurrence of relatively strong signals in the aliphatic region.[32]

^{13}C Photo-CIDNP MAS NMR on Natural Abundance R26 RCs of *Rb. sphaeroides*. Trace A in Figure 6 is the dark spectrum of a n.a. R26 RC sample (shown in black), and trace B shows the evolution of the nuclear polarization in the R26 RC within the first 800 μs. In the initial stage, as shown in the spectrum obtained with a delay time of 0 μs (shown in red), the signal has maximum intensities for both signs and, furthermore, strong positive and negative features appear in the aliphatic region between 0 and 60 ppm. During evolution, the intensity of the entire spectrum decays, and the signals in the aliphatic region disappear entirely (shown in blue). After 100 μs, the resulting spectrum is very similar to that obtained in steady-state experiments (trace C in Figure 6).[16,17] The signal in n.a. R26 RCs is about 20 times stronger than that in n.a. WT RCs having the same concentration. This is due to differences in optical transparency for green laser light between the two samples caused by the absorption of the carotenoid.

Nuclear Polarization Dynamics toward Steady State for R26 RCs. In previous work, steady-state photo-CIDNP signals have been traced back to the TSM, DD, and DR mechanisms.[15,17] To understand the transient signals, polarization in the singlet and triplet branches of the photocycle have to be considered separately. Level mixing by the secular hyperfine interaction in conjunction with *g* value differences Δg leads to nuclear polarization in the singlet branch that is positive for donor nuclei with positive hyperfine coupling and positive Δg. This polarization is exactly offset by polarization with the same amplitude and opposite sign from RCs in the triplet branch. Both contributions together can be considered as antiphase polarization of the singlet state S and the triplet substate T_0.

Shortly after the laser pulse, for a large fraction of RCs in the triplet branch, the donor is still in the triplet state. This leads to strong paramagnetic line broadening, which suppresses NMR signals from this fraction of RCs. The NMR signals from RCs in the singlet branch are then not completely offset by signals from the triplet branch. Transient signals are thus observed, which are entirely due to secular state mixing and stem exclusively from RCs in the singlet branch (Figure 2). In contrast, the steady-state signals stemming from the TSM and DD mechanisms are induced by pseudosecular level mixing, which is generally much weaker than the secular mixing. Therefore, shortly after the laser pulse, the secular transient contribution to NMR line intensities dominates.

The secular mixing is driven by both the isotropic hyperfine coupling a_{iso} and the secular part of the anisotropic coupling

TABLE 5: Polarization of Selected ^{13}C Nuclei in P$_M$, P$_L$, and Φ in Natural Abundance *Rb. sphaeroides* R26 as a Function of the Time Delay between the Light Pulse and the NMR Detection Pulse^a

	normalized NMR intensities					
time delays (µs)	IUPAC no. C19-P$_M$ 163.1 ppm	IUPAC no. C10-Φ 100.7 ppm	IUPAC no. C7^1-P$_L$ 24.1 ppm	IUPAC no. C6-P$_L$ 164.1 ppm	C9-P$_L$ 160.8 ppm	C15-P$_M$ 106.8 ppm
0	0.50	−0.21	0.32	0.63	1.00	−0.35
10	0.51	−0.20	0.31	0.55	0.77	−0.28
100	0.39	−0.15	0.10	0.35	0.61	−0.20
200	0.31	−0.11	0.03	0.28	0.49	−0.15
400	0.33	−0.11	0.01	0.30	0.46	−0.15
800	0.30	−0.09	−0.01	0.32	0.44	−0.16

^{a} Nuclear polarization evolution is plotted in Traces A−A′, Figure 7.

$T(3 \cos^2 \theta - 1)$. For the short radical lifetimes and moderate hyperfine couplings in RCs the transient antiphase polarization is roughly proportional to the secular hyperfine coupling $a_{iso} + T(3 \cos^2 \theta - 1)$. For macroscopically disordered samples as used here, the anisotropic contribution cancels in the orientational average, as $\int(3 \cos^2 - 1) \sin \theta \, d\theta = 0$. At short times after the laser pulse, when the secular transient contribution still dominates, signal intensities are thus roughly proportional to the isotropic hyperfine coupling a_{iso}.

The time evolution of photo-CIDNP MAS NMR spectra of R26 RCs is in good qualitative agreement with these theoretical expectations (Figure 7A,A′,B,B′). Simulations of the primary polarization in the S and in the T$_0$ show that, for positive isotropic hf coupling (a_{iso}) in the S, positive (absorptive) polarization is expected for donor nuclei and negative (emissive) polarization for acceptor nuclei, in agreement with Kaptein's sign rule for the RPM.[24] In the donor, for example, nuclei of RCs in the singlet branch have positive nuclear polarization for $a_{iso} > 0$ and $\Delta g > 0$. Such a polarization pattern is indeed found immediately after light excitation when RCs of the triplet decay pathway are still in the ^{3}P, which is not observable by NMR, and only RCs of the singlet decay pathway have returned to the ground state. This leads to the spin-selective observation of transient nuclear polarization (TNP). Examination of the time evolution of individual signal intensities (traces A and A′ in Figure 7) reveals that, on the expected time scale of about 100 µs, the polarization diminishes due to return of the paramagnetic excited ^{3}P to the ground -state having polarization with opposite sign compared to the S. Nevertheless, the type of polarization pattern (positive donor and negative acceptor signals) is retained, as part of the polarization from the T$_0$ has decayed by paramagnetic relaxation in the ^{3}P so that the S polarization is not fully canceled. Signal intensity of aliphatic carbons decays completely. This is also expected, as for these carbons the ΔA is negligible, leading to much weaker paramagnetic relaxation and the absence of contributions from the TSM and DD mechanisms to net polarization. Assuming a triplet lifetime of 80 µs and the same prefactor for the relaxation rates as in ref 42, we obtain good qualitative agreement between experimental (traces A and A′ in Figure 7 and Table 5) and simulated time traces (Traces B and B′ in Figure 7).

Trace D in Figure 6 is the simulated NMR spectrum of computed photo-CIDNP MAS NMR intensities arising in the ground state exclusively from the singlet state S (dashed arrow in Figure 2A).

The matching of sign and relative magnitude of the nuclear polarization observed in the transient spectrum of *Rb. sphaeroides* R26 (red spectrum of Trace B in Figure 6) is remarkable, albeit not perfect. The comparison between expected nuclear polarization and expected isotropic contribution matches well with the real magnitude and orientation of the computed hf

tensors (see Supporting Information). Deviations of the observed amplitude between experiment and simulation are expected due to errors in the DFT computation of hyperfine couplings and uncertainties in the experimentally determined magnetic parameters of the radical pair (g tensors, dipole−dipole coupling tensor, exchange coupling).

Trace E in Figure 6 is the simulated spectrum considering photo-CIDNP intensities built up by TSM and DD and DR mechanisms in the ground state at the end of the photocycle when both S and T$_0$ polarizations have completely decayed to the ground state.[17]

Evidence for a Fraction of Long-Living Carotenoid Triplet States. The observations on WT RCs are in line with the kinetic scheme in Figure 2B. Because the triplet lifetime of ∼100 ns is much shorter than the duration of the NMR detection pulse of 5 µs, the selective observation of the transient polarization of the S states would not be expected. However, an initial polarization pattern similar to that in R26 RCs occurs with a decay constant of ∼7.5 µs (traces C−C′ in Figure 7 and Table 6). The decay constant coincides with the lifetime of carotenoid triplets under our experimental conditions.[43] Therefore, these results can be explained by assuming that in the presence of the electronic paramagnetic state of the carotenoid, formed by triplet transfer from ^{3}P, nuclear polarization in the triplet branch is transiently obscured by paramagnetically enhanced transverse nuclear relaxation. This enhanced relaxation broadens the NMR lines in the triplet branch beyond detection, so that the corresponding lines in the singlet branch with opposite sign of the intensity become observable. After decay of the ^{3}Car to the ground state, the NMR lines in RCs from the singlet and triplet branch have the same width and the signals with opposite sign cancel. Note that this effect can be described by an average lifetime of ^{3}Car, as it is observable by optical experiments. Different lifetimes of the triplet sublevels, as observable with optically detected magnetic resonance,[44] are not directly manifest in our data. However, some heterogeneity in the lifetime of ^{3}Car is indicated by the fact that only a relatively small fraction of the RCs exhibits this effect.

Transiently obscured polarization (TOP) occurs on Φ during the lifetime of ^{3}P in R26 RCs as well as on P and Φ during the lifetime of the ^{3}Car in WT RCs. There is no experimental evidence for generation of nuclear polarization on the carotenoid itself. In fact, because there is no radical pair involving the carotenoid, polarization from the TSM, DD, and DR mechanisms is not expected. Significant paramagnetic enhancement of transversal nuclear relaxation in P and Φ in the presence of ^{3}Car is likely, as the geometric arrangement of the three chromophores is optimized for orbital overlap. The idea that these signals originate from suppression of the contribution of the triplet branch is supported by their transient character and

Electron−Nuclear Spin Dynamics in Bacterial RCs

J. Phys. Chem. C, Vol. 113, No. 23, 2009 **10277**

TABLE 6: Polarization of Selected ¹³C Nuclei in P_M, P_L, and Φ in 4-ALA *Rb. sphaeroides* Wild Type as a Function of the Time Delay between the Light Pulse and the NMR Detection Pulse[a]

	normalized NMR intensities					
time delays (μs)	IUPAC no. C11-P_L 153.3 ppm	IUPAC no. C19-P_L 159.8 ppm	IUPAC no. C19-Φ 170.0 ppm	IUPAC no. C13-P_M 132.6 ppm	IUPAC no. C6-P_L 164.0 ppm	IUPAC no. C8-Φ 54.6 ppm
0	−0.13	−0.26	0.15	−0.30	−0.15	−0.21
3	−0.23	−0.44	0.12	−0.23	−0.35	−0.17
5	−0.30	−0.55	0.12	−0.19	−0.49	−0.15
7	−0.35	−0.62	0.10	−0.17	−0.58	−0.12
10	−0.40	−0.75	0.09	−0.13	−0.70	−0.08
15	−0.50	−0.91	0.09	−0.09	−0.89	−0.07
30	−0.53	−0.92	0.08	−0.06	−0.85	−0.03
40	−0.52	−0.97	0.07	−0.04	−0.89	−0.01
80	−0.64	−1.00	0.05	−0.05	−0.97	0.00

[a] Nuclear polarization evolution is plotted in Traces C−C′, Figure 7.
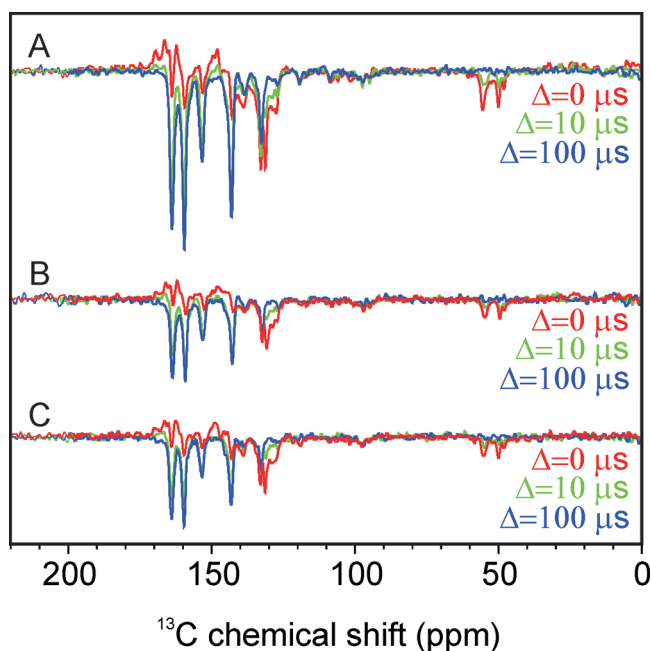
Figure 8. ¹³C photo-CIDNP MAS NMR spectra of RCs of 4-ALA labeled *Rb. sphaeroides* wild type collected using laser pulses at wavelengths of (A) 756 nm, (B) 803, and (C) 860 nm, which are the maximum absorption wavelengths of the bacteriopheophytins, of the accessory bacteriochlorophylls and of donor bacteriochlorophylls, respectively. Colored traces in A, B, and C are three spectra each obtained at different time delays between the light pulse and the NMR detection pulse (red 0 μs, green 10 μs, and blue 100 μs) using 8 ns flashes. All the spectra have been collected at a magnetic field of 4.7 T and a temperature of 233 K.

by the agreement of the polarization pattern with the one expected for the singlet branch.

Nanosecond-flash photo-CIDNP MAS NMR spectra collected using different near-infrared excitations, which directly excite the bacteriochlorophyll and bacteriopheophytin cofactors, demonstrate that the carotenoid triplet in WT RCs obscures triplet branch polarization and thus causes transient appearance of signals from the singlet branch independently of the excitation wavelength (Figure 8). When P is directly excited, photo-CIDNP build-up kinetics is identical to excitation with green light (Trace B in Figures 4 and 5). Therefore, we rule out that direct light absorption by the carotenoid is the cause of the observed transient signals. Simulations of the TOP (traces D−D′ in Figure 7) are in semiquantitative agreement with the experimental results if this fraction is in between 8 and 12%. It is possible that this fraction originates from the carotenoid in the

15,15′-*cis* configuration, while for the 13,14-*cis* conformer, the triplet may decay faster to the ground state.[45] For simulations of the TOP effect in a frozen sample of WT RCs, an average lifetime of the triplet carotenoid is sufficient, as population of any sublevel would lead to signal broadening in the special pair.

Conclusion

In conclusion, we have shown that electron−nuclear spin dynamics in the solid state depends on ΔA (TSM and DD and DR). In addition two transient effects have been discovered. (i) TNP is the observation of nuclear polarization arising selectively from the S. (ii) TOP is induced by nearby triplet excited states and delays triplet polarization detection. Time-resolved photo-CIDNP MAS NMR has also been demonstrated to elucidate the spin dynamics of spin-correlated radical pairs at the atomic resolution and at microsecond time scales. The time-resolved approach presented in this paper allows to determine the map of the electron spin density of the primary photosynthetic radical pair at atomic resolution. In addition, the new insights into the generation of permanent nuclear polarization and of transient signals may help in understanding mechanisms of other solid-state hyperpolarization MAS NMR techniques.

Supporting Information Available: DFT calculation of ¹³C hyperfine tensors, the *g* tensor of the donor *P* and the primary acceptor Φ, the electron−electron dipolar coupling, and the exchange parameter *J*. This material is available free of charge via the Internet at http://pubs.acs.org.

References and Notes

(1) Hoff, A. J.; Rademaker, H.; Van Grondelle, R.; Duysens, L. N. M. *Biochim. Biophys. Acta* **1977**, *460*, 547−554.
(2) Blankenship, R. E.; Schaafsma, T. J.; Parson, W. W. *Biochim. Biophys. Acta* **1977**, *461*, 297−305.
(3) Boxer, S. G.; Chidsey, C. E. D.; Roelofs, M. G. *J. Am. Chem. Soc.* **1982**, *104*, 2674−2675.
(4) Hoff, A. J. *Q. Rev. Biophys.* **1981**, *14*, 599−665.
(5) Hoff, A. J. *Q. Rev. Biophys.* **1984**, *17*, 153−282.
(6) Chidsey, C. E. D.; Takiff, L.; Goldstein, R. A.; Boxer, S. G. *Proc. Natl. Acad. Sci. U.S.A.* **1985**, *82*, 6850−6854.

(7) Kaptein, R.; Oosterhoff, J. L. *Chem. Phys. Lett.* **1969**, *4*, 195–197.

(8) Closs, G. L.; Closs, L. E. *J. Am. Chem. Soc.* **1969**, *91*, 4549–4550.

(9) Bargon, J.; Fischer, H.; Johnson, U. *Z. Naturforsch., A: Phys. Sci.* **1967**, *22*, 1551–1555.

(10) Bargon, J.; Fischer, H. *Z. Naturforsch., A: Phys. Sci.* **1967**, *22*, 1556–1562.

(11) Goldstein, R. A.; Boxer, S. G. *Biophys. J.* **1987**, *51*, 937–946.

(12) Jeschke, G.; Matysik, J. *Chem. Phys.* **2003**, *294*, 239–255.

(13) Polenova, T.; McDermott, A. E. *J. Phys. Chem. B* **1999**, *103*, 535–548.

(14) Zysmilich, M. G.; McDermott, A. *J. Am. Chem. Soc.* **1994**, *116*, 8362–8363.

(15) Prakash, S.; Alia, A.; Gast, P.; de Groot, H. J. M.; Jeschke, G.; Matysik, J. *J. Am. Chem. Soc.* **2005**, *127*, 14290–14298.

(16) Zysmilich, M. G.; McDermott, A. *J. Am. Chem. Soc.* **1996**, *118*, 5867–5873.

(17) Prakash, S.; Alia, A.; Gast, P.; de Groot, H. J. M.; Matysik, J.; Jeschke, G. *J. Am. Chem. Soc.* **2006**, *128*, 12794–12799.

(18) Roy, E.; Alia, A.; Gast, P.; van Gorkom, H.; de Groot, H. J. M.; Jeschke, G.; Matysik, J. *Biochim. Biophys. Acta* **2007**, *1767*, 610–615.

(19) Roy, E.; Rohmer, T.; Gast, P.; Jeschke, G.; Alia, A.; Matysik, J. *Biochemistry* **2008**, *47*, 4629–4635.

(20) Matysik, J.; Alia, A.; Gast, P.; van Gorkom, H. J.; Hoff, A. J.; de Groot, H. J. M. *Proc. Natl. Acad. Sci. U.S.A.* **2000**, *97*, 9865–9870.

(21) Alia, A.; Roy, E.; Gast, P.; van Gorkom, H. J.; de Groot, H. J. M.; Jeschke, G.; Matysik, J. *J. Am. Chem. Soc.* **2004**, *126*, 12819–12826.

(22) Diller, A.; Roy, E.; Gast, P.; van Gorkom, H. J.; de Groot, H. J. M.; Glaubitz, C.; Jeschke, G.; Matysik, J.; Alia, A. *Proc. Natl. Acad. Sci. U.S.A.* **2007**, *104*, 12767–12771.

(23) Volk, M.; Aumeier, G.; Langenbacher, T.; Feick, R.; Ogrodnik, A.; Michel-Beyerle, M. E. *J. Phys. Chem. B* **1998**, *102*, 735–751.

(24) Kaptein, R. *Chem. Commun.* **1971**, 732–733.

(25) Daviso, E.; Jeschke, G.; Matysik, J., *Photo CIDNP MAS NMR.* Aartsma, T. J., Matysik, J., eds.; Springer: Dordrecht, 2008; Vol. II, pp 385−399.

(26) Jeschke, G. *J. Chem. Phys.* **1997**, *106*, 10072–10086.

(27) Schweiger, A.; Jeschke, G. *Principles of Pulse Electron Paramagnetic Resonance*; Oxford University Press: New York, 2001.

(28) McDermott, A.; Zysmilich, M. G.; Polenova, T. *Solid State Nucl. Magn. Reson.* **1998**, *11*, 21–47.

(29) Solomon, I. *Phys. Rev.* **1955**, *99*, 559–565.

(30) Schulten, E. A. M.; Matysik, J.; Alia, A.; Kiihne, S.; Raap, J.; Lugtenburg, J.; Gast, P.; Hoff, A. J.; de Groot, H. J. M. *Biochemistry* **2002**, *41*, 8708–8717.

(31) Prakash, S.; Alia, A.; Gast, P.; de Groot, H. J. M.; Jeschke, G.; Matysik, J. *Biochemistry* **2007**, *46*, 8953–8960.

(32) Daviso, E.; Diller, A.; Alia, A.; Matysik, J.; Jeschke, G. *J. Magn. Reson.* **2008**, *190*, 43–51.

(33) Stoll, S.; Schweiger, A. *J. Magn. Reson.* **2006**, *178*, 42–55.

(34) Diller, A.; Prakash, S.; Alia, A.; Gast, P.; Matysik, J.; Jeschke, G. *J. Phys. Chem. B* **2007**, *111*, 10606–10614.

(35) Veshtort, M.; Griffin, R. G. *J. Magn. Reson.* **2006**, *178*, 248–282.

(36) Stowell, M. H. B.; McPhillips, T. M.; Rees, D. C.; Soltis, S. M.; Abresch, E.; Feher, G. *Science* **1997**, *276*, 812–816.

(37) van Lenthe, E.; Wormer, P. E. S.; van der Avoird, A. *J. Chem. Phys.* **1997**, *107*, 2488–2498.

(38) Huber, M. *Photosynth. Res.* **1997**, *52*, 1–26.

(39) Klette, R.; Torring, J. T.; Plato, M.; Möbius, K.; Bönigk, B.; Lubitz, W. *J. Phys. Chem.* **1993**, *97*, 2015–2020.

(40) Dorlet, P.; Rutherford, A. W.; Un, S. *Biochemistry* **2000**, *39*, 7826–7834.

(41) Matysik, J.; Schulten, E.; Alia, A.; Gast, P.; Raap, J.; Lugtenburg, J.; Hoff, A. J.; de Groot, H. J. M. *Biol. Chem.* **2001**, *382*, 1271–1276.

(42) Prakash, S. Photo-CIDNP studies on reaction centers of *Rhodobacter sphaeroides.* Ph.D. Thesis. Leiden University, 2006; https://openaccess.leidenuniv.nl/dspace/handle/1887/9744/items-by-author?author=Prakash%2C+Shipra.

(43) Angerhofer, A.; Bornhauser, F.; Aust, V.; Hartwich, G.; Scheer, H. *Biochim. Biophys. Acta* **1998**, *1365*, 404–420.

(44) Hoff, A. J. *Metallobiochemistry, Part D* **1993**, *227*, 290–330.

(45) Wirtz, A. C.; van Hemert, M. C.; Lugtenburg, J.; Frank, H. A.; Groenen, E. J. J. *Biophys. J.* **2007**, *93*, 981–991.